J3.1 EVALUATION OF MEANDER-LIKE WIND VARIANCE IN HIGH-RESOLUTION WRF MODEL SIMULATIONS OF THE STABLE NOCTURNAL BOUNDARY LAYER

Nelson L. Seaman*, Brian Gaudet, Aijun Deng, Scott Richardson, D.R. Stauffer and John C. Wyngaard
Pennsylvania State University, University Park, Pennsylvania

and

Larry Mahrt
Oregon State University, Corvallis, Oregon

1. INTRODUCTION

Mesoscale numerical weather prediction (NWP) models are widely used to provide meteorological inputs for air-quality (AQ) models and atmospheric transport and dispersion (AT&D) models. However, NWP models are known to be one of the largest sources of error in AQ and AT&D applications. One of the most critical shortcomings of these models is their poor performance in predicting highly variable light winds close to the surface in stable boundary layers (SBLs). This problem has far reaching consequences because the shallow depth and weak turbulence of typical SBLs lead to poor dispersion of near-surface plumes. Moreover, because turbulence is so weak in the nocturnal SBL, compared to a convectively unstable boundary layer, horizontal plume dispersion is often dominated by fluctuations at the small end of the mesoscale (mesogamma scale (~2-20 km). Generally, the physics of these shallow mesogamma-scale fluctuations is poorly understood.

In stable conditions, the turbulent buoyancy production term acts to suppress vertical motion, leaving horizontal mesoscale forces the chief source of plume dispersion. In such cases, plumes may remain quite highly concentrated over long distances downwind in the mean wind direction, while exhibiting large changes in direction due to mesoscale forcing at scales wider than the plume width. The resulting plume behavior is often referred to as *meandering* and has been observed in all sorts of locales worldwide. Meandering plumes may exhibit large periodic or irregular oscillations in direction, especially when the mean wind is light. In near-calm conditions the plume may even travel in a looping or nearly circular path. Hanna (1983) concluded the two most probable factors contributing to meandering plume behavior are near-surface density driven currents forced by irregular terrain and transient internal gravity waves aloft moving through the environment.

Historically, NWP models have been ineffective at predicting real meandering flows in the SBL because (1) model resolution has been too coarse to resolve the terrain irregularities and mesogamma scale motions that dominate fluctuating wind components in the SBL, and (2) turbulence parameterizations often are poorly designed and inadequately tested for stable conditions. In this study we attempt to explore the limits of SBL predictability and meandering plume behavior at very fine mesoscale resolutions. To meet this objective model evaluation must focus on the mesogamma scale and local plume scale, neither of which is resolved by the standard synoptic meteorological observing network. Thus, model evaluation must span all scales from the synoptic scale to the plume scale. This is an ambitious effort requiring advanced numerical modeling tools and specially designed local observing systems to augment the standard meteorological database.

* *Corresponding author address*: Nelson L. Seaman, Penn State Univ., Dept. of Meteorology, University Park, PA 16802; e-mail: seaman@ems.psu.edu

2. NUMERICAL MODEL AND EXPERIMENT DESIGN

The NWP model chosen for this research is the Weather Research and Forecast (WRF) system known as Advanced Research WRF(i.e., ARW) version 2.2 (Skamarock et al. 2005). WRF-ARW is designed with options for high-order spatial differencing on the Arakawa-C grid, which can be important for numerical accuracy in highly complex flows, especially at very fine resolutions. For this work we choose the fifth-order finite-differencing advection scheme for horizontal advection, the third-order scheme for vertical advection and the third-order Runge-Kutta scheme for temporal integration. These odd-order differencing schemes are designed to maximize the accuracy of small-scale waves (Wicker and Skamarock 2002).

To study the evolution of SBL flow, WRF-ARW is configured with a set of five nested-grid domains, each domain having one-way interaction with the next smaller grid. Table 1 gives the grid resolutions and number of horizontal points in each domain, while Figure 1 shows the location of the domains. All five domains have 41 layers in the vertical. The lowest 5 layers have a depth of 2 m each, after which the layer thicknesses gradually increase with height up to the model top at 50 hPa. This configuration provides 10 layers in the lowest 50 m above ground level (AGL) (Figure 2). The very fine vertical resolution near the surface is designed to resolve SBL structure and processes. The finest domain covers ~67 X 67 km, has a horizontal resolution of 444 m and is centered over the Nittany Valley of central PA (Figure 3). This region is dominated by narrow quasi-parallel ridges oriented southwest-to-northeast, which flank broad valleys, with the Allegheny Mountains located in the northwest part of the domain.

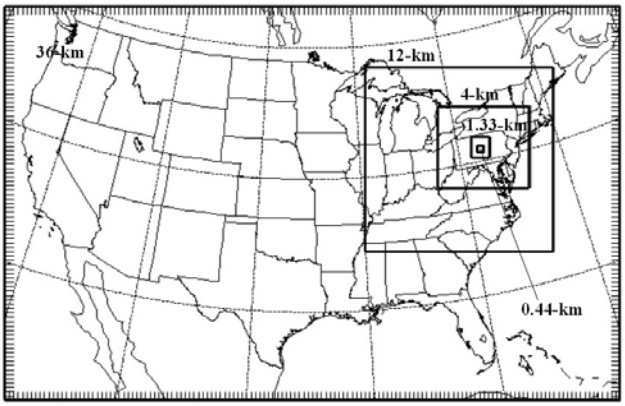

Figure 1. Five-domain nested grid configuration of WRF.

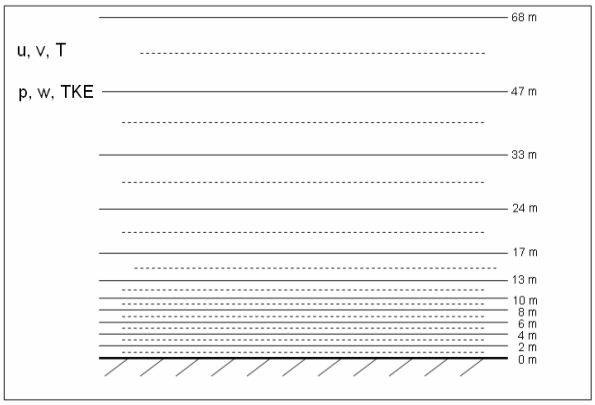

Figure 2. WRF vertical configuration below 70 m AGL.

Domain No.	Horiz. Res. (km)	No. of Points
1	36.0	141 X 91
2	12.0	130 X 127
3	4.0	193 X 169
4	1.333	121 X 121
5	0.444	151 X 151

Table 1. Resolution and size of the five nested-grid WRF domains. All domains have 41 layers in vertical.

This model configuration is designed specifically for investigations of predominantly stable conditions. Vertical and horizontal scaling considerations are based on typical nocturnal SBLs generally having depths on order of h ~ 50 m or less, roughly the thickness of the lowest layer in most general-use mesoscale models. Thus, our horizontal grid scale is ~10 times the depth of the nocturnal SBL (h), while the vertical grid provides up to 10 layers within the typical scale depth of h. Consequently, an ensemble-mean turbulence scheme can be used, similar to those in traditional coarse-resolution mesoscale models for convectively unstable planetary boundary layer (PBL) conditions. Here we choose the Mellor-Yamada-Janjic (MYJ) scheme in WRF (Janjic 2002), which is designed to simulate turbulence for both stable and unstable conditions and has undergone extensive evaluations in research and operations. Other physics for these WRF experiments include the Dudhia radiation scheme and the MM5 five-layer soil scheme for surface fluxes. However, we note that this very fine grid would not be suitable for unstable conditions with a PBL depth > 1 km because the largest eddies would be resolvable and a Smagorinsky-type sub-grid filter scheme would be needed, transforming the model into a large eddy simulation (LES).

The WRF configuration described above is run daily during the nocturnal period for 12 h, beginning at 0000 UTC. The time step on the innermost domain is 2 s. A 12-h model forecast is completed in about 9 h using only four nodes of a Linux cluster at Penn State University (PSU), each node having four 3-GHz CPUs. Output files are saved at 12-minute intervals to provide for analysis of the short-term fluctuations that are resolvable in the very high resolution model.

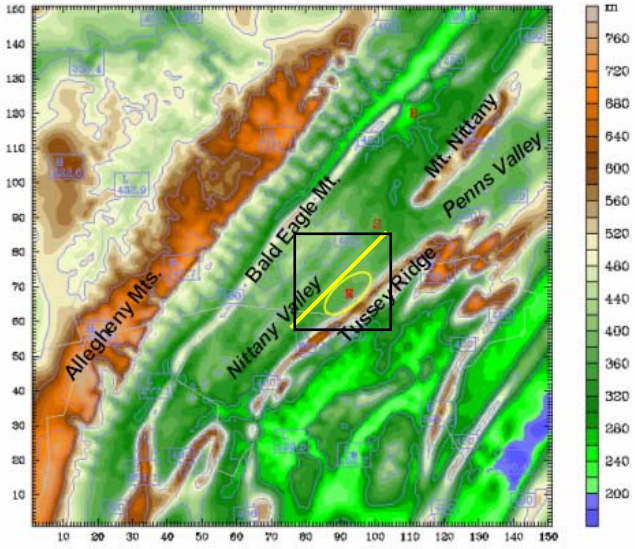

Figure 3. Topography of WRF on Domain 5, horizontal resolution 444 m. Oval marks site of local obs network.

3. LOCAL OBSERVING NETWORK

The very fine grid resolution described in Section 2 is necessary to resolve the fine-scale terrain features expected to dominate internal gravity-wave initiation, near-surface winds in the Nittany Valley (Figure 3) and the vertical structure of the SBL. However, to evaluate the WRF model's potential for predicting low-level advection in the SBL, including meandering wind behavior, it is critical to obtain high-resolution wind and temperature data in the valley. Most prior field studies aimed at studying PBL characteristics have had spatial distributions, instrumentation types or sampling rates not well designed for studying the SBL. Thus, a network of instrumented towers is being installed in a gently rolling section of Nittany Valley known as Rock Springs, close to the northwest base of Tussey Ridge (see yellow ellipse, Figure 3). This valley site is ideal for our purposes because the quasi-linear ridge-and-valley topography of central PA makes it easier to separate the role of regional versus local terrain forcing. Also, the

rolling topography of the Nittany Valley is typical of most regions within the Eastern U.S.

Wind speed and direction at Rock Springs are measured using Vaisala WS425 two-dimensional sonic anemometers. These instruments have a very low starting threshold (~0.05 ms^{-1}), one-second sampling time, very low power requirements and no moving parts. In late summer 2007 the first five sonic anemometers were deployed in a preliminary "scoping" network on 10 m towers at elevations of 3 and 10 m AGL, along with thermistors for measuring temperature. Each tower is outfitted with a battery powered data recorder and a transmitter which relays the data to a central network computer for preliminary quality checking and formatting. The battery packs are solar rechargeable to provide continuous operation. Once collected the raw data are averaged to one-minute values prior to distribution to users and archival. Additional instrument deployments are planned in stages for early 2008.

4. MODEL RESULTS AND EVALUATION

4.1 *Vertical Structure of the SBL*

As a first step toward model evaluation, we have examined the ability of the MYJ turbulence parameterizetion and high-resolution WRF-ARW configuration to predict realistic vertical structure of the SBL. Since the scoping field network is incomplete, the evaluations are largely qualitative at present. However, this is a necessary first step intended to guide further development of the field network and numerical model investigations.

Figure 4 shows a fairly typical nocturnal warm-season skew-T log p sounding for central PA predicted by WRF at Rock Springs at 0300 UTC, 10 Sept. 2007. The sounding shows the shallow SBL (very stable layer close to the surface) having a depth of ~40 m. The winds in Figure 4 (right) indicate very strong directional shear in and just above this layer, with speeds between 0.75-1.5 ms^{-1} in the lowest 100 m AGL. Between 40–250 m there is a weaker inversion layer where cool air has filled most of the Nittany Valley almost to the height of the flanking ridges. Above the inversion lies a nearly adiabatic remnant of the prior daytime convective PBL.

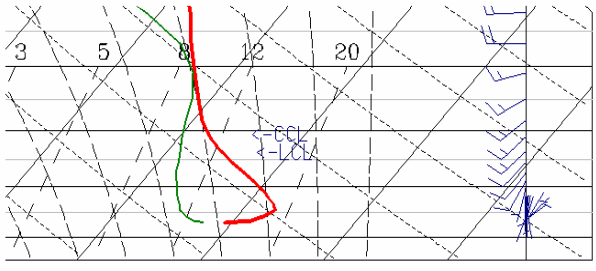

Figure 4. Skew-T log p diagram based on 3-h WRF-ARW prediction at Rock Springs, PA, 0300 UTC, 10 Sept. 2007.

Next, Figures 5 and 6 compare near-surface buoyancy flux profiles predicted by WRF-ARW at Rock Springs, PA, in the 10 Sept. case versus an observed 1-h averaged profile from the CASES99 study reported by Vickers and Mahrt (2004), respectively. In their study Vickers and Mahrt showed that buoyancy flux in the SBL often decreases more or less linearly with height from a strongly negative value at the surface to a small value at the top of the SBL. Above the SBL the flux profile often approaches a constant even if there is turbulence aloft. They concluded the SBL depth can be diagnosed in many cases as the level where the absolute value of the flux stops decreasing, which can be very useful when turbulence exists through a deep layer further aloft. However, we note there can be many exceptions where other processes can disrupt this "ideal" profile, such as when wind shear in the base of a nocturnal low-level jet (LLJ) generates turbulence aloft,

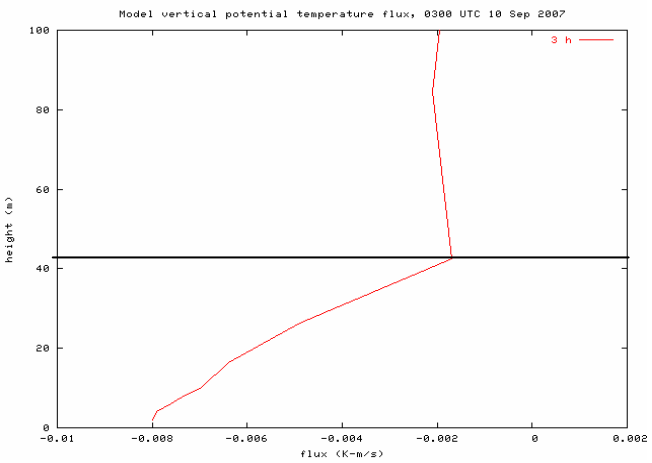

Figure 5. Vertical profile of buoyancy flux (Kms^{-1}) forecast by WRF-ARW at Rock Springs, PA, 0300 UTC, 10 Sept. 2007. Horizontal line is diagnosed SBL depth.

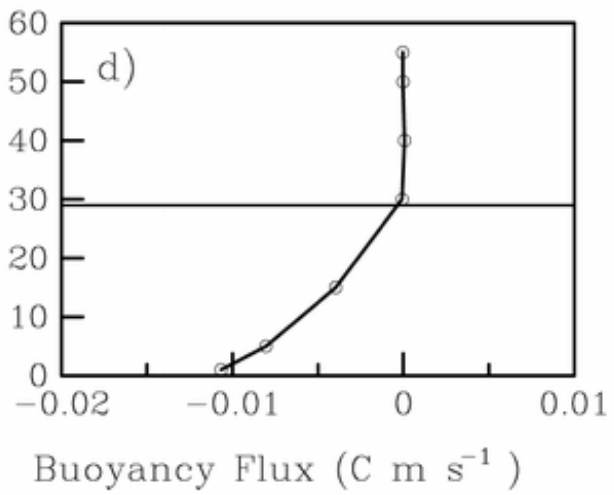

Figure 6. Same as Figure 5, except for observed 1-h averaged buoyancy flux from CASES99, 18 Oct. 1999.

which then can be transported downward toward the surface. In Figure 5 the model-predicted buoyancy flux profile is very similar to the ideal case of Vickers and Mahrt, even though there is slight negative flux above the diagnosed SBL top. In this case the small flux aloft is probably related to weak vertical mixing in and below the residual mixed layer between ~250-1500 m AGL. Planned future deployment of thermistors and anemometers at multiple levels on a 50-m tower should allow direct verifications of model-predicted buoyancy flux profiles. Meanwhile, given the apparent effectiveness of the MYJ PBL scheme and high-resolution WRF configuration for predicting realistic SBL structure, a prototype diagnostic algorithm has been written to analyze SBL depth routinely from WRF output.

Figure 7 demonstrates this diagnostic nocturnal SBL depth, along with potential temperature and turbulent kinetic energy (TKE), in a vertical cross section through a portion of the Nittany Valley near Rock Springs at 0800 UTC, 14 November 2007. In this cool-season case, the SBL depth is only ~15-30 m deep. While TKE is minimal near the surface, there is considerable TKE aloft in part of the cross section where wind shear is sufficient to generate modest instability. At other times (not shown) downward transport of the turbulence from aloft causes intermittent episodes of greater turbulence intensity in the layers near the surface. In those cases the concept of a definable shallow SBL may be replaced by a continuously turbulent zone extending temporarily from the surface up to several hundred meters. When the shear aloft subsequently decreases sufficiently, the elevated TKE weakens or dissipates, allowing the shallow radiation-driven SBL to become re-established. Thus, the model appears capable of simulating commonly observed nocturnal turbulence behavior.

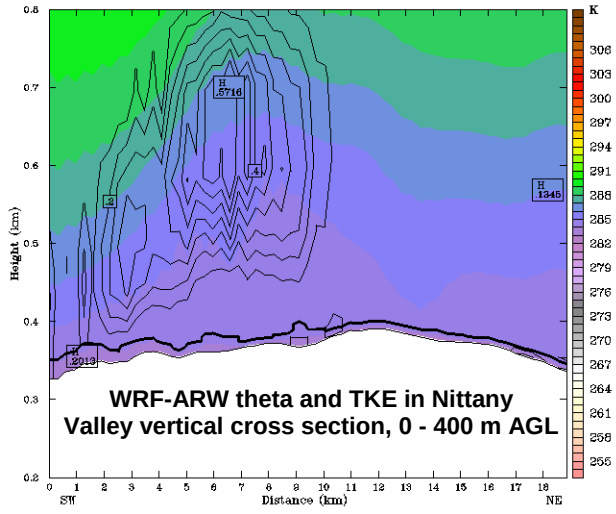

Figure 7. Predicted 8-h potential temperature (K, color fill) and turbulent kinetic energy (m^2s^{-2}, thin solids) on the WRF-ARW 0.444-km domain in a vertical cross section (lowest 500 m) parallel to axis of Nittany Valley, at 0800 UTC, 14 Nov. 2007. Heavy solid line indicates diagnosed SBL depth. Cross section location in Fig. 3.

4.2 *Internal Gravity Waves and Surface Density Flow*

Density-driven currents are common near the surface on clear nights due to radiative cooling over sloping terrain. In mountainous regions these density currents are referred to as mountain breezes, but they are ubiquitous over small hills and gentle slopes as well, especially when the mean wind is weak. Internal gravity waves can be induced in the stable free atmosphere by a variety of forcing mechanisms that cause vertical displacement of the horizontal flow. Perhaps the most common wave-inducing mechanism involves lifting of a stably stratified current over a ridge or mountain range. These so-called mountain-wave events generate gravity waves propagating in both the vertical and horizontal directions. In the lee of major mountain ranges such as the Rockies and Alps, they can induce intense turbulent rotors (Grubisic et al. 2004) or strong downslope winds (Klemp and Lilly 1975) called Chinooks or foehns.

Internal gravity waves also are common over and downwind of the various ranges of the Appalachian Mts. Depending on vertical stability, these waves may propagate predominantly in the vertical, resulting in a single mountain wave, or else mostly in the horizontal as a train of trapped lee waves. Lee wave trains are common downwind from the Allegheny Mountains in PA and can occur in any season, but they are most often observed in the cold season when stability is large through a deep layer of the troposphere.

Figure 8 shows an example of a train of trapped internal gravity waves in the lee of the Allegheny Mountains predicted by the WRF-ARW on a 100X100 point sub-section of the 1.33-km domain at 0900 UTC, 18 August 2007. The wavelength of the lee-wave train

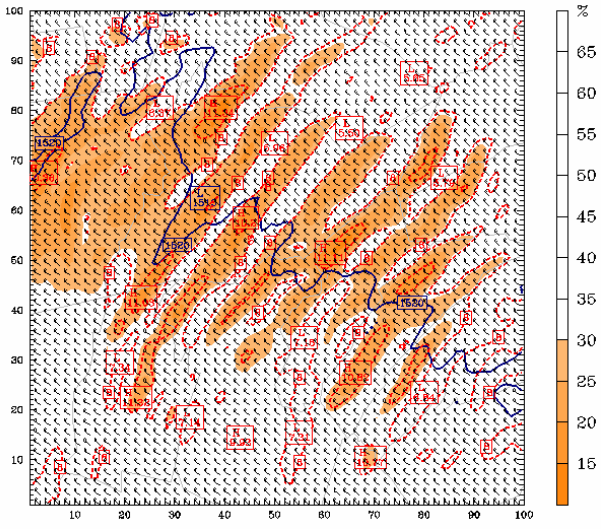

Figure 8. WRF-predicted 850-hPa wind (ms^{-1}) and relative humidity (%, color fill) at +9 h on a 100 X 100 point sub-section of the 1.33-km domain, valid for 0900 UTC, 18 Aug. 2007.

in this post-cold-front case is ~14 km and the wind above 950 hPa is northwesterly at ~15 ms^{-1}. Examination of the corresponding WRF solution on the 4-km domain for the same case (not shown) reveals that these waves are poorly resolved by the coarser grid and thus are "aliased" to longer wavelengths, as expected. However, Figure 9 shows that the waves propagate smoothly from the 1.33-km domain into the 0.444-km domain, preserving their wavelength and amplitude quite well, while avoiding significant distortion or refraction along the domain interfaces.

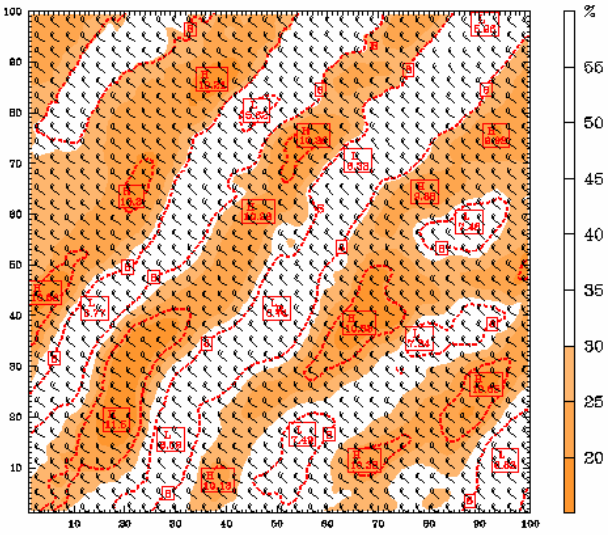

Figure 9. Same as Figure 8, but for a 100X100 subsection of the 0.444-km domain.

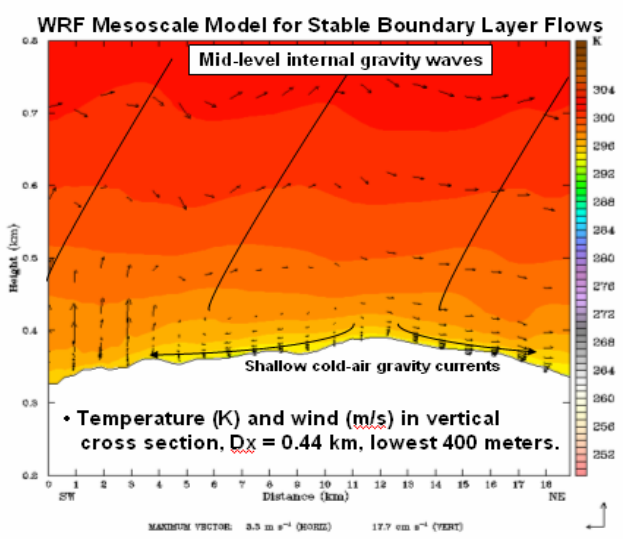

Figure 10. Potential temperature (K, color fill) and wind vectors (arrows) predicted by WRF-ARW on the 0.444-km domain in a vertical cross section (lowest 500 m) parallel to axis of Nittany Valley, 0900 UTC, 14 Aug. 2007. Heavy solid lines indicate gravity wave axes (aloft) and direction of near-surface density driven currents. Cross section location shown in Figure 3.

Without remote sensing instrumentation to observe the flow aloft over central PA in the region where the waves are propagating, it is difficult to verify the model prediction in this case, especially since the dryness of the atmosphere prevents the development of orographic clouds. However, in the case of 7 November 2007, trapped wave clouds having wavelengths of ~10-11 km were observed by visible GOES-East satellite images (not shown) in a stratocumulus cloud deck near 850 hPa. These mid-level wave-induced clouds confirm a similar lee wave train predicted by WRF-ARW at the same level and having the same wavelength. These and similar results from other cases verify that the high-resolution WRF configuration is able to predict the basic characteristics of internal gravity waves generated by the narrow Allegheny Mountain range which frequently impact the study area.

Next, Figure 10 reveals the vertical structure of propagating model-predicted internal gravity waves in the case of 14 August 2007, when the mean winds aloft were more gentle (~5 ms^{-1}) and from the southwest. The waves in Figure 10 are evidenced by perturbations in the potential temperature and vector wind fields in the region above the ridge tops (~300 m above the terrain of the valley floor shown in the figure), but they also extend downward to the surface where their amplitude is damped. Close to the ground, cool density-driven currents are shown propagating downhill both to the southwest (left) and northeast (right) in the figure. Thus, the WRF-ARW is simultaneously generating perturbed flow through the physical processes hypothesized by Hanna (1983) to induce low-level wind fluctuations that, in light-wind conditions, can result in plume meandering.

4.3 *Statistical Evaluation on Mesoalpha Scale*

Evaluation of WRF-ARW for SBL conditions also must determine the model's accuracy for predicting the synoptic and mesoalpha scales. Large errors on these outer domains will inevitably cause error growth on the innermost domains, as well. Statistical evaluation was performed using the Model Evaluation Toolkit (MET) code provided by the WRF Development Testbed Center (DTC) in Boulder, CO. MET was set up to run automatically following each model forecast cycle and can calculate a wide range of statistics commonly used for NWP model verification, plus advanced object-oriented statistics. The forecasts are validated against standard surface METAR and radiosonde data. Here we focus on domain-averaged root mean square error (RMSE) and mean error (ME, or bias) for surface temperature and wind. Evaluations using MET are conducted only on the outer three domains (36, 12 and 4 km) because the finer domains contain too few observations to obtain reliable domain-wide statistics.

Figures 11 and 12 present samples of the temporal evolution of RMSEs and Bias errors for 2-m temperatures and 10-m winds, respectively, predicted in the case of 7 November 2007. Figure 11 shows that the RMSEs for surface temperatures on the 12-km domain

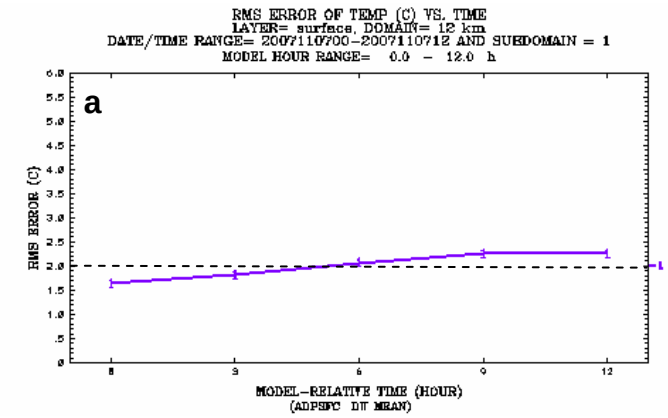

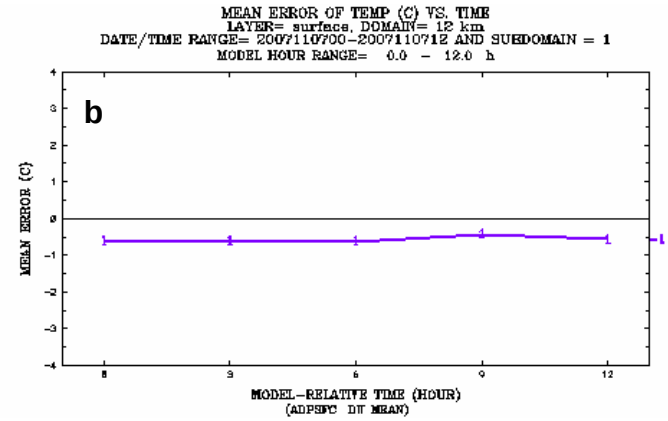

Figure 11. Temporal evolution of WRF-ARW 12-km domain-averaged statistics for 2-m temperature (C), 0000-1200 UTC, 7 Nov. 2007. (a) RMSE, (b) Bias error.

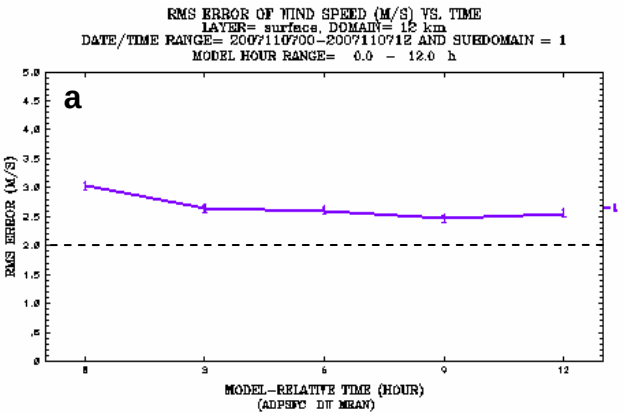

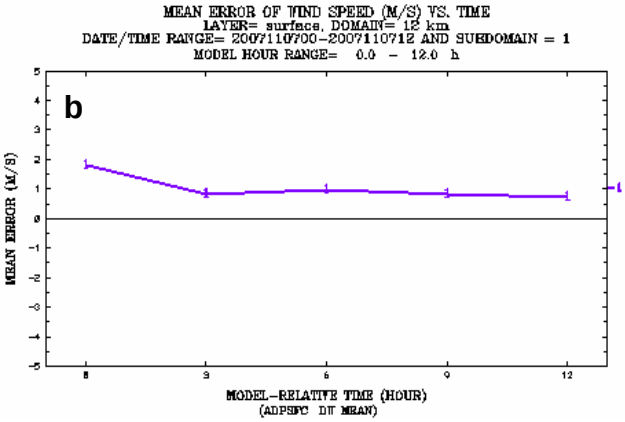

Figure 12. Temporal evolution of WRF-ARW 12-km domain-averaged statistics for 10-m wind speed (ms^{-1}), 0000-1200 UTC, 7 Nov. 2007. (a) RMSE, (b) Bias error.

are ~2 C, rising very slowly through the 12-h forecast. In fact, the initial conditions, which are interpolated from NCEP's Global Forecast System (GFS) analyses, contain a RMSE of ~1.85 C. The corresponding bias error for surface temperature is ~ -0.5 C and is virtually unchanged through the forecast period. Meanwhile, the RMSE for wind speed actually drops from ~3 ms^{-1} in the initial analysis to ~2.5 ms^{-1} by +9 h, while the wind bias falls to less than 1 ms^{-1} over the same interval (Figure 12). Statistics for the 36-km and 4-km domains are quite similar (not shown).

The domain-averaged vertical profiles of RMSEs and bias errors for wind and temperature also were examined for the 36-, 12- and 4-km grids (not shown). They indicate WRF-ARW errors in these cases are similar or lower than to those reported for winter season-averaged WRF forecasts reported by Koch and Gall (2005) (not shown). While the sample statistics presented here are for only one case, scripting is currently being added to allow the user to composite the daily statistics for many cases during a specified period, which will provide a much more representative assessment of mesoalpha-scale model accuracy.

4.4 *Local Fluctuations and Meandering Winds*

The final step of this preliminary model evaluation involves verification of local winds and temperatures predicted by WRF-ARW at Rock Springs, PA, where the scoping field network is located. Since plume transport and dispersion is the cumulative result of integrated wind and turbulence acting on air parcels, it is important to examine the fluctuating component of the predicted low-level state variables in addition to their means.

We begin by comparing the observed wind speed and direction to the model-predicted speed and direction at Tower Site 1, which is located about 0.75 km from the base of Tussey Ridge at Rock Springs (~2.5 km southwest of "R" in Figure 3). Figure 13 shows the observed and predicted wind speed at 3 m and 10 m AGL on the night of 7 October 2007. The speeds are plotted as one-minute averages and thus may contain some fluctuations on time scales too short for the WRF model to simulate well. However, the dominant non-turbulent fluctuations appear to have periods of ~0.5-2.0 h. The mean observed wind speed is initially ~1.5 ms^{-1} at Site 1, but quickly falls to ~0.4-0.6 ms^{-1}, thereafter rising to 1.0-2.5 ms^{-1} about 1000-1200 UTC. Figure 13a

also reveals there is some modest speed shear between 3 and 10 m AGL, as expected.

Figure 13b indicates that WRF predicts a mostly similar evolution of SBL wind speed during the nocturnal period of 7 October 2007. The model's winds are also one-minute averages, not than instantaneous outputs, to ensure against the possibility that non-physical high-frequency numerical noise might contaminate results. After initial adjustments, low-level speeds are predicted to be ~1.0-2.0 ms^{-1}, followed by weaker speeds of ~0.6-1.0 ms^{-1} in the middle of the night and higher speeds of ~1.0-2.2 ms^{-1} between 1000-1200 UTC. Of special interest are the speed fluctuations having periods of ~0.5-2.0 h. Similar to the observations, the highest amplitude speed fluctuations occur near the initial time and again in the last several hours of the 12-h forecast. Clearly, these fluctuations occur on time scales much too long to be associated with the small turbulent eddies in the SBL. Rather, we hypothesize that these periodic fluctuations are associated primarily with the passage of mid-level internal gravity waves propagating through the model atmosphere, as shown in Figure 10.

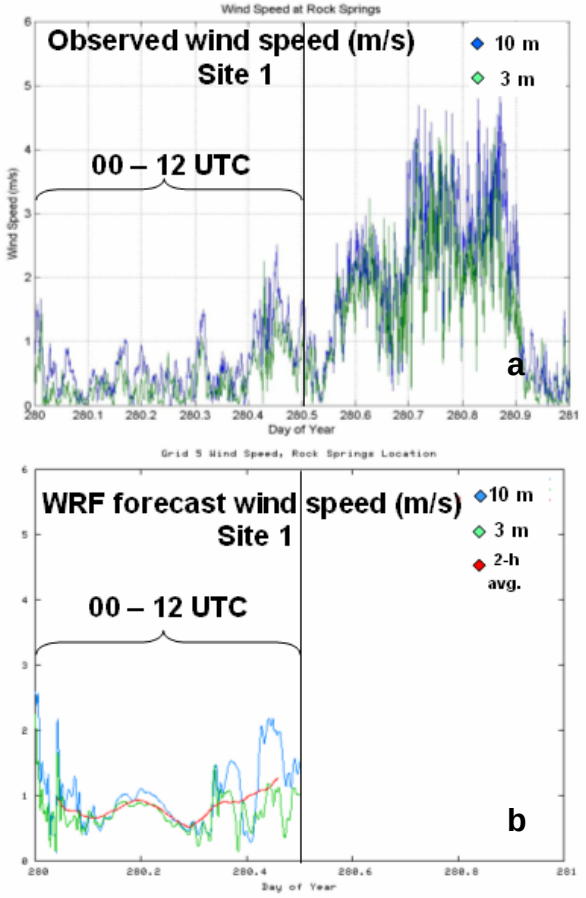

Figure 13. Comparison of (a) observed and (b) forecasted wind speeds (ms^{-1}) at Site 1, Rock Springs, PA, for the period 0000-1200 UTC, 7 October 2007. Red shows 2-h running mean for model prediction, based on average of 3-m and 10-m winds.

Next, Figure 14 shows a similar comparison for 12-minute averaged nocturnal wind directions observed and forecasted for the night of 7 October at Site 1 near the base of Tussey Ridge. The observed winds have a mean direction of ~210 degrees through most of the night, with large fluctuations of about +/- 100 degrees. The south-southwesterly mean direction is oriented roughly parallel to the ridges flanking Nittany Valley. Wind rose analysis based on nocturnal winds at Site 1 during 4-25 October 2007 (not shown) indicates the most frequent directions at Site 1 range from 195-255 degrees (southwesterly), with a secondary maximum from 135-165 degrees (south-southeasterly). Thus, the mean direction on 7 October is typical for this site. The frequent short episodes of southeasterly flow evident through most of the night may be related to pulses of density-driven winds moving down the slopes of nearby Tussey Ridge.

However, Figure 14b also reveals that the WRF predicted a mean nocturnal wind direction of ~250 degrees. This represents an error in mean wind direction at Site 1 of ~40 degrees. Visual inspection of model-predicted flow near Rock Springs on other nights having light winds and a well-developed shallow SBL

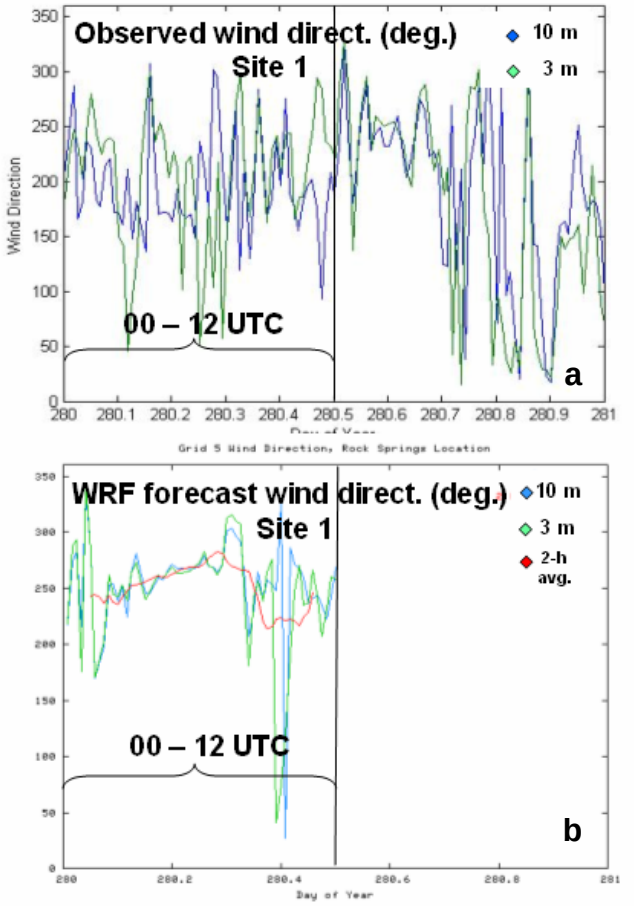

Figure 14. Same as Figure 13, but for (a) observed and (b) forecasted wind directions (deg).

suggest that mean southwesterly flows in Nittany Valley are quite common in the model. Hence, it seems that the direction error in the 7 October case is likely to be non-systematic, but obviously possible, at least for this site. With the further development of post-processing analysis software, investigations over many cases will help determine what model errors are typical for the focus region. Meanwhile, Figure 14b shows that directional fluctuations in WRF-ARW for this night also are about +/-100 degrees, on the same scale as those observed in Figure 14a. However, given the model's very small time steps (2 s), they definitely cannot be attributed to numerical "noise." We note that very few previous numerical investigations have been able to generate fluctuations of predicted speed and direction on time scales shorter than an hour in a manner having any apparent relationship to observations. These non-turbulent fluctuations are critical to understanding and predicting realistic plume behavior in stable light-wind conditions, including plume meandering.

Figure 15 presents the corresponding observed and model-predicted temperatures at Site 1 through the night of 7 October 2007. Note that the temperatures observed at 2 m AGL are about 2 C cooler than those at 9 m AGL, indicating a very strong near-surface inversion in the SBL. This is about twice the thermal inversion predicted by WRF-ARW in Figure 15b. However, the greatest error in the model prediction for this case is that the cooling rate during the early evening is much too weak. Further examination of the model initial conditions revealed that the GFS analysis for 2-m temperature was 2.0-2.5 C too cold over PA, with even larger errors at 9 m AGL. Similar errors were found in the NCEP GFS 0000 UTC analyses of 2-m temperatures for many cases during the late summer of 2007. However, these large analysis errors disappeared or were greatly diminished after mid-October following the introduction of several code modifications to the GFS software at NCEP.

Insight into the net effect on transport due to wind fluctuations in the SBL can be gained by examining parcel trajectories. Figure 16 presents a plot of 4-h trajectories for nine parcels released in one grid cell at Rock Springs, PA, from a height of 5 m AGL at 0800 UTC, 14 August 2007. Without sub-grid dispersion the cluster of parcels moves toward the northeast carried by the mean southwesterly low-level winds (~1 ms^{-1}) in the SBL. This direction is consistent with the most frequent directions observed in the valley, as discussed above. However, due to the periodic fluctuations in wind direction, many of the parcels move in a sinusoidal manner characteristic of a classic meandering plume. As expected in real cases, this behavior is not universal. Some of the parcels, released nearby within the same grid cell, move in a more-or-less straight path toward the northeast. Examination of near-surface trajectories on other nights having light winds and at other sites across Nittany Valley reveal a host of wandering-parcel responses, including near-circular looping, direction reversals and meandering (not shown).

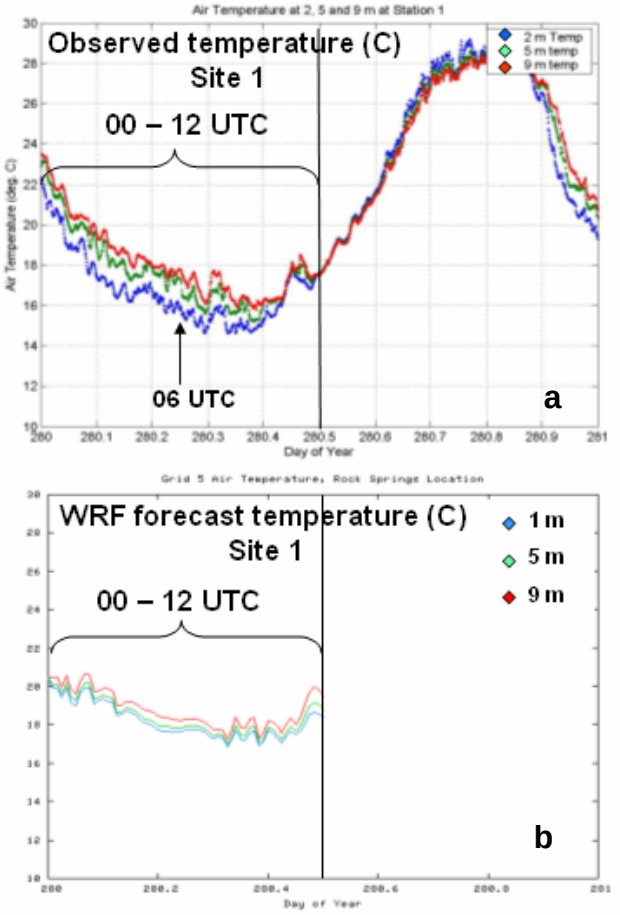

Figure 15. Same as Figure 13, except for three levels of (a) observed and (b) forecasted temperatures (C).

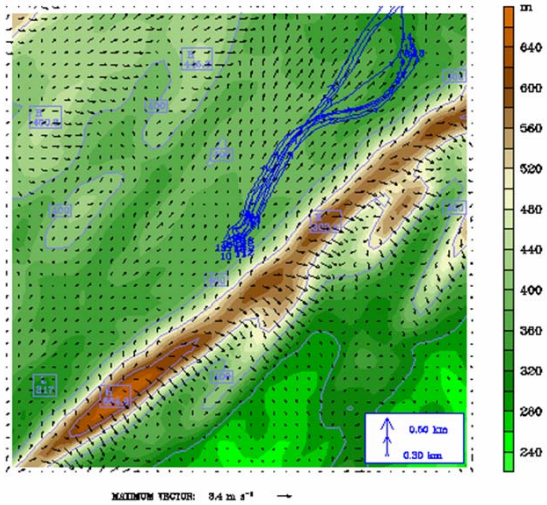

Figure 16. Meandering trajectories in Nittany Valley (0800-1200 UTC) for nine parcels released near Rock Springs at 5 m AGL and wind vectors at 1200 UTC, 14 Aug. 2007, on a 0.444-km sub-domain of WRF-ARW. Sub-domain location shown in Figure 3.

Finally, Figure 17 presents a sample of plume transport with dispersion included, based on the WRF-predicted 0.444-km meteorology and calculated using the SCIPUFF AT&D model (Sykes et al 1993; 1998). In this case the plume is released from the Rock Springs Site 1 at a height of 1 m AGL at 0800 UTC, 14 August 2007. The figure presents cumulative surface dosage of an inert tracer received at the surface over the following four hours. Transported by the meandering south-westerly flow, the plume dosage spreads northeastward until it encounters Mt. Nittany (see Figure 3). Thereafter, due to the strong stability in the shallow SBL, the plume splits into two branches, one proceeding northeastward down the Nittany Valley and the other heading east-northeastward into Penns Valley. Vertical cross sections through the plume (not shown) indicate virtually all of the released material remains below 100 m AGL with little "leakage" above the SBL. Qualitatively, this seems to be fairly realistic behavior, although no tracer data are available to confirm the prediction.

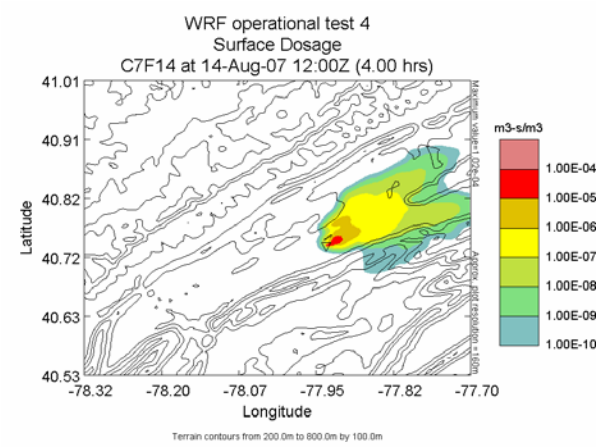

Figure 17. SCIPUFF AT&D prediction of surface dosage for an inert tracer released from Rock Springs, PA, at 1 m AGL, 0800 UTC, 14 Aug. 2007.

5. SUMMARY

In this study, a newly instrumented field network and specially configured version of the WRF-ARW NWP model have been used to study predictability of SBL structure and behavior. Using very fine grid resolution and the MYJ PBL scheme, it has been shown that the modeling system can predict important aspects of the nocturnal SBL, including realistic buoyancy flux profiles and wind speed and direction fluctuations responsible for low-level plume meandering.

Future expansion of the field network will provide additional towers, including one up to 50 m. PSU also is investigating options for remote sensing to monitor internal gravity-wave activity aloft. Additional work will extend the multi-scale model evaluations to include testing of the Quasi-Normal Scale Elimination (QNSE) PBL scheme of Galperin et al. (2007).

Acknowledgements: This research has been sponsored by the Defense Threat Reduction Agency under contract no. W911NF-06-1-0439-MOD-P00001. We also acknowledge the Development Testbed Center in Boulder, CO, for providing assistance with its MET codes and Mr. Glenn Hunter of Penn State for assistance with a number of the figures.

6. REFERENCES

Galperin, B., S. Sukoriansky and V. Perov, 2007: Implementation of the quasi-normal scale elimination (QNSE) turbulence model in WRF. 8th WRF Users Workshop. Boulder, CO, 11-15 June.

Grubisic, V., J. Doyle, J. Kuettner, G.S. Poulos and C.C. Whiteman, 2004: T-REX: Terrain-Induced Rotor Experiment overview document and experimental design. 72 pp. Available at http://www.eol.ucar.edu/projects/trex/documents/TREX_SOD.pdf.

Hanna, S.R., 1983: Lateral turbulence intensity and plume meandering during stable conditions. *J. Clim. Appl. Meteor.,* **22**, 1424-1430.

Janjic, Z.I., 2002: Nonsingular implementation of the Mellor-Yamada Level 2.5 Scheme in the NCEP Meso model. NCEP Office Note 437, 61 pp. Available online at http://www.ncep.noaa.gov.

Klemp, J.B., and D.K. Lilly, 1975: The dynamics of wave-induced downslope winds. *J. Atmos. Sci*., **32**, 320-339.

Koch, S.E. and R. Gall, 2005: The DTC Winter Forecast Experiment: Final Project Report. Available from Development Testbed Center, Boulder, CO, 27 pp.

Skamarock, W.C., J.B. Klemp, J. Dudhia, D.O. Gill, D.M. Barker, W. Wang and J.G. Powers, 2005: A description of the advanced research WRF version 2. NCAR Tech. Note NCAR/TN-468+STR, 88 pp.

Sykes, R.I., S.F. Parker, D.S. Henn and W.S. Lewellen, 1993: Numerical simulations of ANATEX tracer data using a turbulence closure model for long-range dispersion. *J. Appl. Meteor*., **32**, 929-947.

Sykes, R.I., S.F. Parker, D.S. Henn, C.P. Cerasoli and L.P. Santos, 1998: PC-SCIPUFF version 1.2 PD technical documentation. ARAP Report 718, 170 pp.

Vickers, D. and L. Mahrt, 2006: Evaluating formulations of stable boundary layer height. *J. Appl. Meteor*., **43**, 1736-1749.

Wicker, L.J., and W.C. Skamarock, 2002: Time splitting methods for elastic models using forward time schemes. *Mon. Wea. Rev*., **130**, 2088-2097.